




# Exploring metal ion metabolisms to improve xylose fermentation in *Saccharomyces cerevisiae*

Gisele Cristina de Lima Palermo,<sup>1,2</sup>  Natalia Coutouné,<sup>1,2</sup>  João Gabriel Ribeiro Bueno,<sup>1,2</sup> Lucas Ferreira Maciel<sup>1</sup> and Leandro Vieira dos Santos<sup>1,2</sup> 

<sup>1</sup>Brazilian Biorenewable National Laboratory (LNBR), Brazilian Center for Research in Energy and Materials (CNPem), Campinas, São Paulo 13083-100, Brazil.

<sup>2</sup>Genetics and Molecular Biology Graduate Program, Institute of Biology, University of Campinas (UNICAMP), Campinas, São Paulo, Brazil.

## Summary

The development of high-performance xylose-fermenting yeast is essential to achieve feasible conversion of biomass-derived sugars in lignocellulose-based biorefineries. However, engineered C5-strains of *Saccharomyces cerevisiae* still present low xylose consumption rates under anaerobic conditions. Here, we explore alternative metabolisms involved in metal homeostasis, which positively affect C5 fermentation and analyse the non-obvious regulatory network connection of both metabolisms using time-course transcriptome analysis. Our results indicated the vacuolar Fe<sup>2+</sup>/Mn<sup>2+</sup> transporter *CCC1*, and the protein involved in heavy metal ion homeostasis *BSD2*, as promising new targets for rational metabolic engineering strategies, enhancing xylose consumption in nine and 2.3-fold compared with control. Notably, intracellular metal concentration levels were affected differently by mutations and the results were compared with positive controls *isu1Δ*, a Fe-S cluster scaffold protein, and *ssk2Δ*, a component of HOG pathway. Temporal expression profiles indicate a metabolic remodelling in response to xylose, demonstrating changes in the main sugar sensing signalling pathways.

## Introduction

The increasing environmental concerns regarding energy production from fossil sources have driven the

development of cleaner alternatives to restructure the global energy matrix. A renewable and environment-friendly alternative to produce fuels and chemicals is the use of lignocellulosic biomass, a plant-derived feedstock essentially composed of cellulose (40–60%), hemicellulose (20–40%) and lignin (10–24%) (Sharma *et al.*, 2019). The cellulose and hemicellulose fractions are mainly constituted of glucose (C6) and xylose (C5) monosaccharides and the maximum conversion by microbial platforms into higher added value bioproducts is essential for the feasibility of lignocellulose-based biorefineries.

The budding yeast *Saccharomyces cerevisiae* is the commonly eukaryotic organism used in industrial bio-based processes due to its robustness against several stresses (Attfield, 1997). However, although this yeast excels in fermenting glucose, wild type strains are unable to ferment pentose sugars as xylose, requiring synthetic biology strategies towards integration of heterologous metabolic pathways (Moysés *et al.*, 2016). Two different xylose consumption pathways are commonly used to engineer a yeast cell: the oxidoreductive (OXR) pathway, which converts xylose to xylulose by an oxo-reduction reaction catalysed by two enzymes, xylose reductase (XR) and xylitol dehydrogenase (XDH); and the xylose isomerase (XI) pathway, which consists in a single-step reaction catalysed by the XI enzyme, encoded by *xylA*. Since XI does not require redox cofactors necessary for XR/XDH activity, the use of the isomerase pathway does not lead to a cellular redox imbalance present on the OXR alternative, being a more advantageous C5 metabolic route (Kwak and Jin, 2017). However, although *xylA* expressing strains achieve higher ethanol yields (Li *et al.*, 2016), it still presents low anaerobic xylose consumption rates, demanding further genetic modifications to increase strain's performance. Other modifications, such as overexpression of genes from pentose phosphate pathway (PPP), deletion of the aldose reductase *GRE3* or expression of heterologous transporters can be a relevant approach to improve strain fitness (Bueno *et al.*, 2020).

Newly arising beneficial mutations fixed in cell population during evolution experiments are frequently off-pathway and can be a promising approach to explore molecular basis and alternative metabolisms that positively affect fitness in anaerobic C5 fermentation (Zhou *et al.*, 2012; Qi *et al.*, 2015;). Recently, evolutionary engineering studies revealed a strong selective pressure

Received 30 March, 2021; accepted 25 June, 2021.

For correspondence. E-mail leandro.santos@lnbr.cnpem.br; Tel. +55 (19) 3518 3124.

*Microbial Biotechnology* (2021) 14(5), 2101–2115  
doi:10.1111/1751-7915.13887

on genes involved in metal homeostasis as deletion of the genes encoding a scaffold protein for mitochondrial iron-sulfur clusters (ISC) biogenesis, the *ISU1*, and a  $\text{Ca}^{2+}/\text{Mn}^{2+}$  Golgi ATPase, the *PMR1* gene, was reported to improve xylose-to-ethanol conversion on *xylA* strains (Santos *et al.*, 2016; Sato *et al.*, 2016; Verhoeven *et al.*, 2017). As XI is a metalloenzyme that requires two divalent metal cations for the isomerization of xylose into xylulose (Kovalevsky *et al.*, 2010; Lee *et al.*, 2017;), changes in intracellular metal homeostasis could enhance XI activity *in vivo* by increasing the availability of cofactors (Lee *et al.*, 2020). Interestingly, deletion of *ISU1* also had a positive effect on an XR/XDH strain (Osiro *et al.*, 2019), suggesting a broader relation of metal homeostasis in improving xylose fermentation through optimization of other metal-dependent enzymes or different pathways of the cell metabolism. Additional gene mutations on the high osmolarity glycerol (HOG) pathway were also described by both studies that found the evolution-based mutations on *ISU1* (Santos *et al.*, 2016; Sato *et al.*, 2016;). The knock-out mutations in the mitogen-activated protein kinase (MAPK) gene, the *HOG1*, and in the *SSK2* gene, encoding an upstream MAPKKK from HOG pathway (Saito and Posas, 2012), were described as capable to improve xylose metabolism on anaerobic conditions, however, few indications on how these mutations could interfere with xylose metabolism have been described (Wagner *et al.*, 2019).

Recently, a mathematical genome-scale metabolic model was constructed to predict responses of metabolism and gene expression upon the availability of metal ions, demonstrating the dependence of enzymes on metal ions and the effect in yeast metabolism on a genome-scale (Chen *et al.*, 2021). Heterologous pathways can be included in the model, amplifying the field for its application in the design and improvement of distinct bioproducts. The model was able to predict the influence of iron in an engineered yeast for biosynthesis of *p*-coumaric acid (*p*-HCA), demonstrating the important application of metal homeostasis in optimization of cell factories to the biotechnological industry and metabolic engineering studies.

In this work, our goal was to provide deeper insights into how different metabolisms related to metal homeostasis could affect xylose fermentation by evaluating uncorrelated genes in a C5 engineered strain. Here, we explore how those mutations affected the yeast xylose fermentation, metal intracellular content, resistance to oxidative stress and gene expression, comparing with the previous phenotypes found on *isu1Δ* and *ssk2Δ* mutant cells. We also explore a global time-course transcriptional profile of *ISU1* deletion to further enlightenment on the molecular mechanisms which allow an enhanced xylose consumption phenotype.

## Results and discussion

### Rational selection of gene targets

To further investigate the hypothesis whether modifications in metabolisms associated with metal homeostasis could impact xylose fermentation, six genes from different metabolic pathways related to metal homeostasis were rationally selected to be deleted on the xylose-consuming strain C5TY (C5-Trial Yeast), a yeast cell designed specifically to screen for mutations related to xylose metabolism. The yeast C5TY has an additional copy of each of the genes encoding a xylulokinase (*XKS1*) and of four genes from PPP (*TAL1*, *RKI1*, *TKL1* and *RPE1*), deletion of *GRE3* and multiple integrated copies of *xylA*.

The choice of the genes targets was based on distinct and distant functions from the genes previously described in the literature (Santos *et al.*, 2016; Sato *et al.*, 2016; Verhoeven *et al.*, 2017) and their function alters the accumulation or intracellular flow of divalent metals as cobalt, manganese, magnesium and iron, which have been reported to be cofactors of XIs (Kovalevsky *et al.*, 2010; Lee *et al.*, 2017; Fig. S1). The genes selected includes *BSD2*, involved in heavy metal homeostasis (Liu *et al.*, 1997); *CCC1*, a vacuolar Fe/Mn<sup>2+</sup> membrane importer (Li *et al.*, 2001); *FRE6*, a ferric reductase (Martins *et al.*, 1998); *HMX1*, a heme oxygenase (Protchenko and Philpott, 2003); *MNR2*, a vacuolar Mg<sup>2+</sup> exporter gene (Pisat *et al.*, 2009); and *SMF3*, a vacuolar Fe<sup>2+</sup> exporter with the opposing function of Ccc1p (Portnoy *et al.*, 2000).

### Genes involved in metal homeostasis impacts xylose fermentation

To assess novel putative metabolisms associated with improved xylose fermentation, single deletions were performed in the background strain C5TY for the selected genes highlighted above and on *ISU1* and *SSK2* genes (as positive controls), which deletions have been previously described to positively affect xylose consumption (Santos *et al.*, 2016; Sato *et al.*, 2016). A double mutant *ccc1Δssk2Δ* was also generated to verify the synergistic effect of these mutations in xylose consumption. Fermentation assays were performed with all mutants (*bsd2Δ*, *ccc1Δ*, *fre6Δ*, *hmx1Δ*, *mnr2Δ*, *smf3Δ*, *isu1Δ* and *ssk2Δ*) and the control, C5TY, in YP-media supplemented with 50 g l<sup>-1</sup> xylose as the sole carbon source. Maximum specific growth rate (h<sup>-1</sup>) and the fermentative parameters ethanol productivity (g l<sup>-1</sup> h<sup>-1</sup>), ethanol yield (g-ethanol/g-xylose) and maximum specific xylose consumption rate (g g<sup>-1</sup> CDW h) were evaluated for all strains (Table 1).

**Table 1.** Fermentation performance of mutants and parental strain C5TY.

Strain	Max. specific growth rate ( $\text{h}^{-1}$ )	Ethanol productivity per hour ( $\text{g l}^{-1} \text{h}^{-1}$ )	Ethanol yield per xylose ( $\text{g g}^{-1}$ )	Max. specific xylose consumption rate ( $\text{g g CDW}^{-1} \text{h}^{-1}$ )	Xylitol yield per xylose ( $\text{g g}^{-1}$ )
C5TY	0.0535	$0.05 \pm 0.00$	$0.33 \pm 0.04$	$0.52 \pm 0.07$	$0.05 \pm 0.01$
<i>smf3Δ</i>	0.0475	$0.03 \pm 0.00$	$0.32 \pm 0.08$ (−0.75%)	$0.29 \pm 0.01$ (−43.20%)	$0.07 \pm 0.02$
<i>mnr2Δ</i>	0.0336	$0.04 \pm 0.00$	$0.22 \pm 0.02$ (−32.83%)	$0.48 \pm 0.02$ (−6.06%)	ND
<i>hmx1Δ</i>	0.0319	$0.09 \pm 0.02$	$0.31 \pm 0.04$ (−6.29%)	$0.54 \pm 0.02$ (4.50%)	ND
<i>fre6Δ</i>	0.0313	$0.10 \pm 0.00$	$0.36 \pm 0.06$ (10.85%)	$0.52 \pm 0.04$ (0.87%)	ND
<i>bsd2Δ</i>	0.0642	$0.11 \pm 0.02$	$0.40 \pm 0.02$ (23.69%)	$0.59 \pm 0.16$ (14.41%)	$0.02 \pm 0.00$
<i>ssk2Δ</i>	0.0619	$0.27 \pm 0.02$	$0.42 \pm 0.00$ (28.01%)	$0.98 \pm 0.13$ (90.61%)	$0.01 \pm 0.00$
<i>ccc1Δ</i>	0.0687	$0.42 \pm 0.01$	$0.43 \pm 0.00$ (31.70%)	$1.08 \pm 0.05$ (109.26%)	$0.01 \pm 0.00$
<i>isu1Δ</i>	0.0936	$0.53 \pm 0.00$	$0.43 \pm 0.00$ (31.58%)	$1.25 \pm 0.10$ (142.08%)	$0.01 \pm 0.00$

ND, not determined.

All cultivations were performed in YPX50 and values represent the averages of three biologic replicates  $\pm$  SD between 0 and 40 h. The percent difference of ethanol yield and maximum specific xylose consumption rate related to C5TY are represented between parentheses.

Consistent with a previous study (Santos *et al.*, 2016), *isu1Δ* strain required only 40 h to consume all xylose present on the medium, exhibiting the highest ethanol productivity ( $0.53 \pm 0.00 \text{ g l}^{-1} \text{h}^{-1}$ ) and xylose consumption rate ( $1.25 \pm 0.10 \text{ g g}^{-1} \text{CDW h}$ ) among all strains (Fig. 1 and Table 1), showing an 11-fold enhancement of xylose fermentation when compared with the control. Deletion of *CCC1*, led to a ninefold increase in ethanol productivity ( $0.42 \pm 0.01 \text{ g l}^{-1} \text{h}^{-1}$ ), surpassing the performance of the previously described *SSK2* loss-of-function mutation (Santos *et al.*, 2016), which achieved an ethanol productivity of  $0.27 \pm 0.01 \text{ g l}^{-1} \text{h}^{-1}$  in this study (Fig. 1 and Table 1). Interestingly, when deletion of *CCC1* and *SSK2* was combined to create the double mutant *ccc1Δssk2Δ*, the resulted strain showed a productivity sixfold higher than the single mutant *ccc1Δ* in 24 h, equalling the performance along with the fermentation (data not shown). Synergistic interaction between *SSK2* and *ISU1* have also been reported to enhance xylose metabolism (Santos *et al.*, 2016).

The strain *bsd2Δ* also presented an increase of 2.3-fold in ethanol productivity compared with the control (Table 1). In contrast, strains harbouring the knockout of *SMF3* and *MNR2* encoding the vacuolar exporters of  $\text{Fe}^{2+}$  and  $\text{Mg}^{2+}$ , respectively, demonstrated the worst performance in xylose among all deletants (Fig. 1 and Table 1), even though both deletants did not decrease glucose growth (data not shown).

Deletion of *HMX1* and *FRE6* showed more subtle changes on xylose fermentation (Table 1), suggesting that those deletions might have a more subtle impact on the cellular iron metabolism under iron-sufficient conditions than the other genes evaluated.

#### Intracellular metal levels were affected differently by mutations

The previously described improvement in xylose utilization due to *PMR1* loss-of-function was associated with the

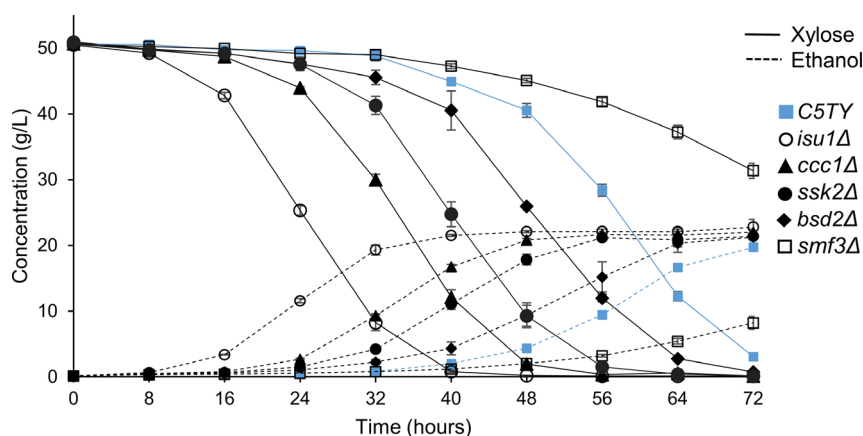


**Fig. 1.** Comparative fermentation profile of selected transformants and control in xylose medium. To analyse the effect of each deletion in the parental strain C5TY, strains were cultivated in YPX in batch-fermentation for 72 h. All fermentations were performed in triplicate and error bars represent standard deviation.

higher intracellular manganese content found in this mutant since the loss of function of *PMR1* increases the cytosolic concentration of  $\text{Ca}^{2+}/\text{Mn}^{2+}$  by disabling their transport from cytosol into the Golgi lumen, increasing the available cofactor levels for *xyIA* activity (Yu *et al.*, 2012; Verhoeven *et al.*, 2017;). Therefore, we speculated if the increase in intracellular metal ions could also trigger the enhancement of xylose consumption found in our strains.

To verify how mutations changed the intracellular metal content, we analysed the intracellular availability of calcium (Ca), cobalt (Co), iron (Fe), magnesium (Mg), manganese (Mn) and zinc (Zn) on the selected strains *isu1Δ*, *ccc1Δ*, *ssk2Δ*, *bsd2Δ* and *smf3Δ* compared with the control C5TY (Fig. 2A). Intracellular amounts of magnesium and zinc did not have expressive changes across the mutant strains when compared with C5TY, while cobalt content had a significant decrease in almost all strains (Student's *t*-test,  $p < 0.05$ ), except in *ccc1Δ*. Interestingly, *ccc1Δ* did not have expressive alterations

in any metal concentration when compared with the control, even though its deletion is known to increase cytosolic amounts of  $\text{Fe}/\text{Mn}^{2+}$  by disabling vacuole storage of these ions (Li *et al.*, 2001).

In contrast, deletion of *BSD2* led to the highest intracellular accumulation of iron and manganese observed across the strains. Even though *BSD2* deletion was reported to accumulate Co, Cd and Mn by increasing membrane stability of the heavy metal transporters Smf1p/Smf2p (Liu *et al.*, 1997; Yu *et al.*, 2012;), in our results even *bsd2Δ* strain showed a decrease in cobalt content compared with the control. Interestingly, it also shows an increase in intracellular iron that was not reported up to date.

Although it has been proposed that Smf3p acts as a  $\text{Fe}^{2+}$  vacuolar importer, *smf3Δ* also led to an increase in manganese content, agreeing with a previous report (Yu *et al.*, 2012). This transporter is part of the family of the same *Nramp* family of transporters of Smf1p/Smf2p,

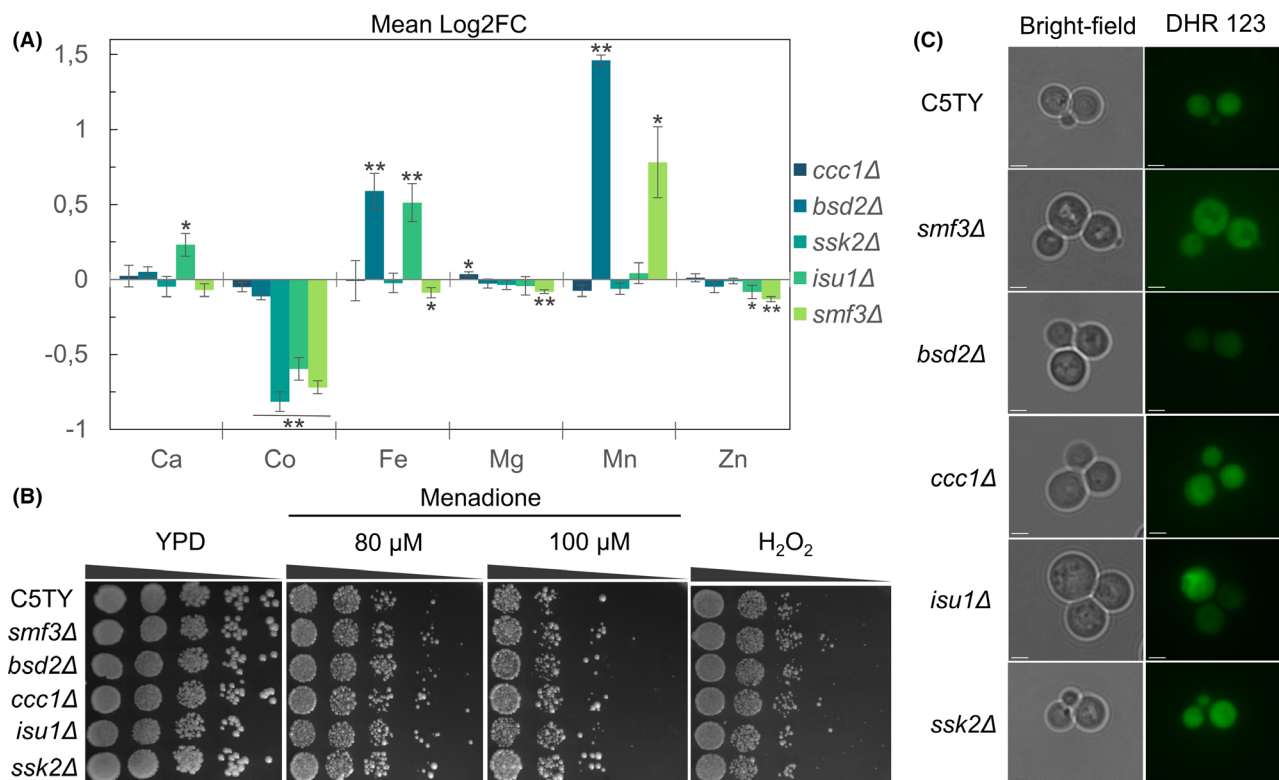


**Fig. 2.** Intracellular metal content and oxidative stress tolerance of transformants and the control C5TY.

A. Mean log<sub>2</sub> fold change of intracellular metal concentration of calcium (Ca), cobalt (Co), iron (Fe), magnesium (Mg), manganese (Mn) and zinc (Zn) of mutants compared with the control C5TY. Statistical analysis was performed by Student's *t*-test and asterisks denote statistically significant differences ( $*P < 0.05$ ,  $**P < 0.01$ ). All data represent the mean of  $n = 3$  biologically independent samples and error bars represent standard deviation.

B. Measurement of cellular generation of ROS by fluorescent microscopy with the dye DHR 123. The scale bar indicates 2  $\mu\text{M}$ .

C. Oxidative stress tolerance assay on solid YPD medium supplemented with 80  $\mu\text{M}$  or 100  $\mu\text{M}$  of Menadione or 3 mM of H<sub>2</sub>O<sub>2</sub>.

which are directly related to manganese homeostasis, suggesting that Smf3p could also be involved in manganese homeostasis. Since *SMF3* deletion disables cells to access its vacuolar storages, it is suggested that besides cellular accumulation, metal ion compartmentalization is an important factor for xylose fermentation in XI-engineered strains.

As described in literature (Garland *et al.*, 1999), *isu1Δ* exhibits an increased amount of iron and, curiously, it also had led to a significant increase in calcium content. On the other hand, *ssk2Δ* did not lead to an increase in intracellular metal concentration. *SSK2* gene encodes an upstream MAPKKK of the HOG signalling pathway involved in the adaptation to high osmolarity stress (Saito and Posas, 2012) and its deletion was reported to lead to a decrease in active Hog1p (Laviña *et al.*, 2014), the kinase effector of the HOG pathway. Although *ssk2Δ* did not change intracellular metal levels, a link between the HOG pathway and iron homeostasis was reported as Hog1p was recently described to negatively regulate the iron uptake by favouring nuclear export of the transcription factor Aft1p (Martins *et al.*, 2018).

#### *Mutations did not impair strain tolerance to oxidative stress*

High levels of metals can be toxic to the cells by the increase of oxidative stress (Morano *et al.*, 2012), which is an undesirable trait to a scale up industrial strategy for engineered strains. Since it was observed changes in intracellular concentration of metal ions and/or its cellular distribution on mutant cells compared with control, a tolerance assay to oxidative stress with menadione or hydrogen peroxide (H<sub>2</sub>O<sub>2</sub>) was done (Fig. 2B) and the generation of cellular reactive oxygen species (ROS) was measured by fluorescent microscopy using the dye dihydrorhodamine 123 (DHR 123; Fig. 2C).

Despite the increase of intracellular metal levels found in the mutants *isu1Δ*, *ccc1Δ*, *ssk2Δ*, *bsd2Δ* and *smf3Δ* strains, the oxidative stress response assay showed no change in ROS levels and growth in the presence of H<sub>2</sub>O<sub>2</sub> and menadione when compared with the control.

#### *Main differences in gene expression started at the beginning of fermentation*

In order to understand the unique fermentation profile of each strain and to identify the main differences of gene expression shown on xylose, exploring individual cellular signatures, solutions and responses of each metabolism, we selected the four-best mutants *isu1Δ*, *ccc1Δ*, *ssk2Δ* and *bsd2Δ*, based on their fitness, productivity and ethanol yield (Table 1), to analyse gene expression patterns and transcriptome profiles through fermentation.

We first compared the mRNA from parental strain, C5TY, with the mutant yeast cells *isu1Δ*, *ccc1Δ*, *ssk2Δ* and *bsd2Δ* at their first sample, corresponding to 8 h after the beginning of the experiment. Although xylose consumption profile at 8 h does not show significant differences between the selected strains (Fig. 1), *isu1Δ* and *ssk2Δ* surprisingly showed large changes in gene expression, presenting 1.199 and 997 differentially expressed genes (DEGs) relative to C5TY (Fig. 3A and B). However, *ccc1Δ* and *bsd2Δ* strains showed only 34 and 37 genes differentially expressed, respectively (Fig. 3C and D).

Among the genes differentially expressed in the strains, deletion of *CCC1* was the only to increase the expression of *GRX4* and *TYW1* genes, encoding a cytosolic monothiol glutaredoxin and an iron-sulfur protein, which protects cells from iron toxicity and is required for synthesis of Wybutosine-modified tRNA (Mühlenhoff *et al.*, 2010; Li *et al.*, 2011;), respectively, remaining upregulated all long of fermentation. Both genes are under the control of the transcription factor Yap5p in iron-replete conditions (Martínez-Pastor *et al.*, 2017), which suggests that *ccc1Δ* cells are sensing high levels of intracellular iron even though this strain did not present significant alterations on intracellular iron concentrations. Since the Ccc1p transporter works in the intracellular distribution of ions and its deletion increases cytosolic amounts of iron (Li *et al.*, 2001), the iron sensed by the mutated cell might be differentially compartmentalized compared with the control.

To characterize the main transcriptional changes at the beginning of fermentation on *isu1Δ* and *ssk2Δ* strains, we performed the functional enrichment analysis of DEGs classified by biological process from gene ontology (GO) terms (<http://www.geneontology.org/>) on each mutant, considering only results for Benjamini-Hochberg corrected p-value < 0.05. Table S1 summarizes the top 10 GO terms classified by their biological process found on DEGs of each mutant strain for 8 h of fermentation.

The GO terms found in *isu1Δ* strain are similar to the transcriptional response to fermentable sugars, such as glucose, expressing upregulated genes enriched mainly in the glycolytic process (GO:0006096) and tRNA aminoacylation for protein translation (GO:0006418), and downregulated genes enriched for nitrogen utilization (GO:0019740), fatty acid beta-oxidation (GO:0006635), mitochondrial gene expression (GO:0140053) and cellular respiration (GO:0045333), suggesting that the transcriptional responses necessary for xylose fermentation were present on *isu1Δ* strain since the beginning of the fermentation. Nevertheless, the term glucose import (GO:0046323), which includes hexose transporters responsible for xylose transport, was also overrepresented among the

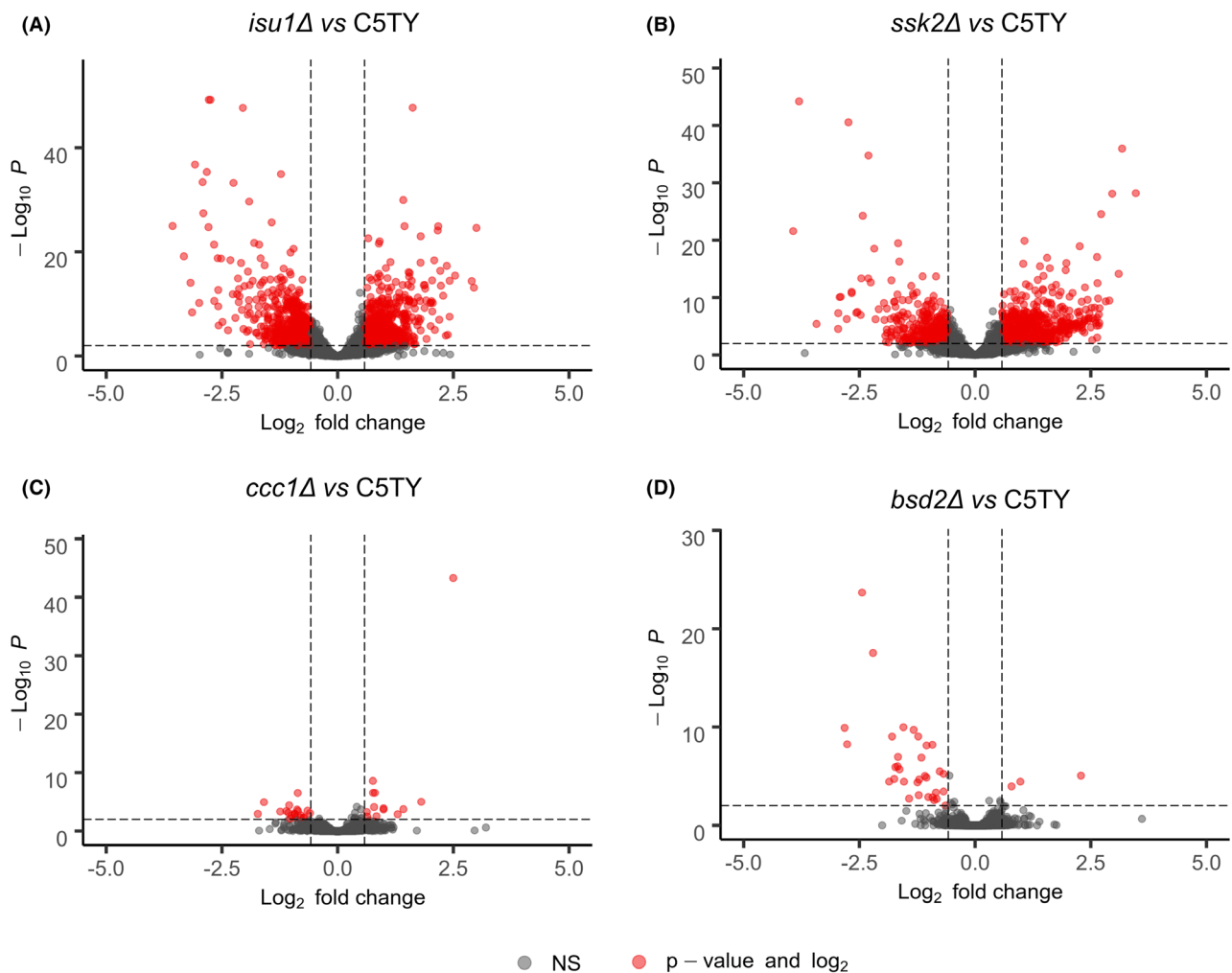


**Fig. 3.** Graphical representation of DEGs at 8 h of fermentation. mRNA from parental strain, C5TY, was compared with the expression of the mutant yeast cells *isu1Δ* (A), *ssk2Δ* (B), *ccc1Δ* (C) and *bsd2Δ* (D) at 8 h of fermentation. Only transcripts with  $FDR < 0.01$  and  $|\log_2FC| > 0.58$  between the compared groups were considered as differentially expressed (red). Non-significant genes are shown in grey. Relative mRNA concentrations were calculated from three independent biological replicates.

downregulated genes, suggesting a non-efficient regulation of the transport system in the presence of this pentose.

In addition, as *ISU1* is involved in mitochondrial iron-sulfur biogenesis, the expression of genes from this metabolism was explored more deeply (Fig. S2). As expected, *isu1Δ* was the only strain with a wide alteration in genes required for cellular iron-sulfur cluster assembly at this time point, exhibiting six genes of this metabolism downregulated (*GRX5*, *ISA1*, *NFS1*, *ISD11*, *CIA2*, *NAR1*) and two genes upregulated (*MET18* and *TAH18*). Interestingly, the strain *ssk2Δ*, which presented the second most DEG profile at 8 h, also presented the upregulation of *MET18* and *TAH18*, indicating the broad application of these genes in cellular metabolism.

On the other hand, the *ssk2Δ* strain showed different GO terms of downregulated and upregulated

genes compared with the *isu1Δ* strain. As Ssk2p plays a role in the HOG stress pathway, its deletion has led to the downregulation of genes involved in different types of stress, such as response to  $H_2O_2$  (GO:0042542), regulation of protein stability (GO:0031647), and cellular response to heat (GO:0034605; Table S1), even though it did not impair the tolerance to oxidative stress of this mutant (Fig. 2B and C). Although *SSK2* deletion has been reported to lead to a decrease in active Hog1p (Laviña *et al.*, 2014), *HOG1* expression in *ssk2Δ* strain did not change compared with the control. Moreover, a HOG-independent function of Ssk2p has been described (Laviña *et al.*, 2014) and thus we could not assume that the phenotype exhibited for *ssk2Δ* was only due to its connection to the HOG pathway.

### Mutations favours the expression of genes required for xylose fermentation

The carbon flux through the PPP and glycolysis is a bottleneck in xylose fermentation. To investigate how the selected mutations altered the yeast primary metabolism, we analysed the temporal expression levels of genes from the central carbon metabolism and aerobic respiration (Fig. 4 and Fig. S3).

In strains in which xylose was completely or almost exhausted from media until 48h (*isu1Δ* and *ccc1Δ*), expression of genes related to the PPP and alcoholic fermentation is correlated with xylose concentration, decreasing its expression as the pentose is consumed from the medium (Fig. 4A and Fig. S3). In contrast, genes involved in the TCA, glyoxylate cycle and aerobic respiration were upregulated only when xylose starts being depleted (Fig. 4B and C and Fig. S3). The

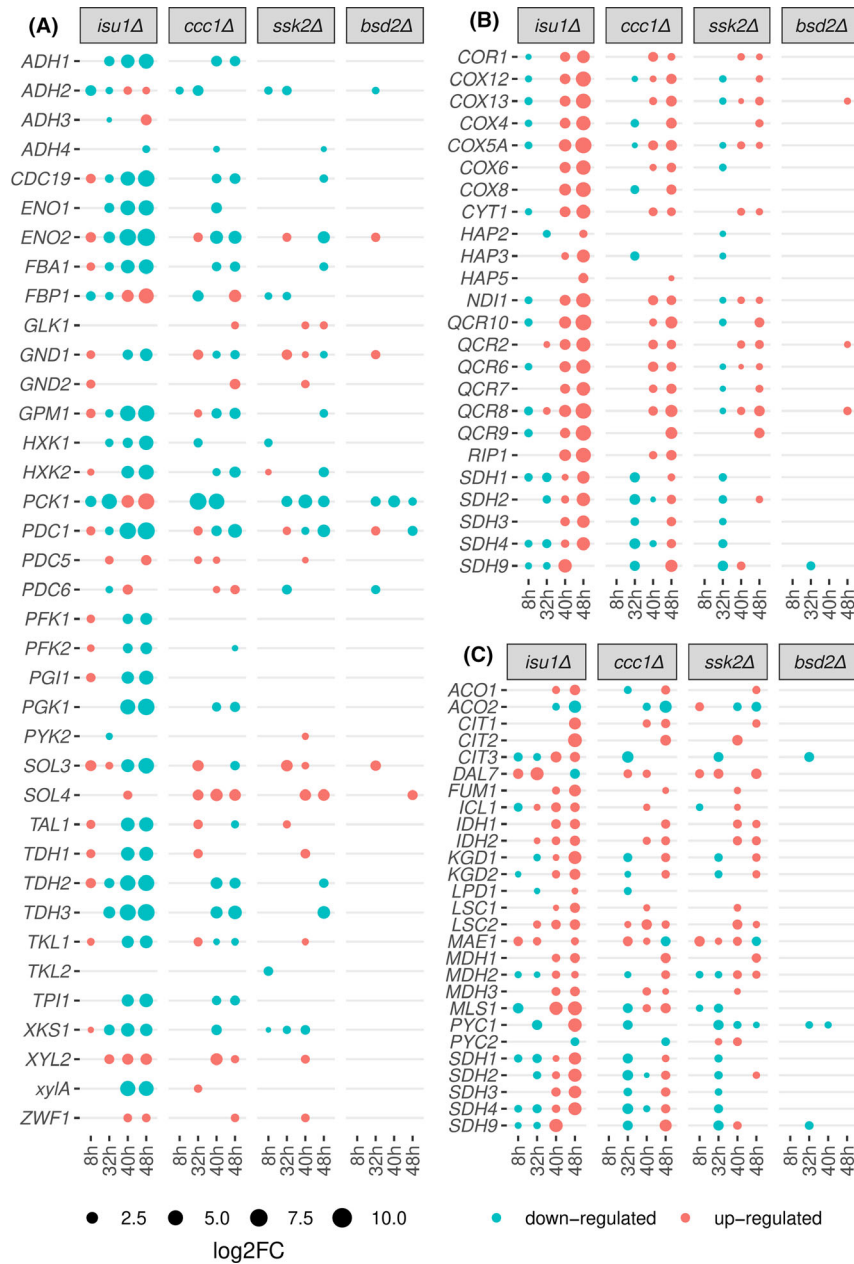


**Fig. 4.** Temporal profiles of genes involved in the central carbon metabolism, aerobic respiration and TCA/glyoxylate cycle in each mutant relative to the control C5TY at specific time-points. Genes from alcoholic fermentation, xylose metabolism and PPP (A), aerobic respiration (B) and TCA and Glyoxylate cycles (C) are represented in this bubbleplot. Colours show up (red) and downregulation (blue) of genes and the bubble size is proportional to average Log<sub>2</sub> fold change values of genes in each time-point compared with its respective time of C5TY.

phosphoenolpyruvate carboxykinase (*PCK1*) and fructose-1,6-bisphosphatase (*FBP1*), gluconeogenesis specific enzymes, were downregulated at the initial fermentation points of almost all strains compared with the control, changing their expression only after the sugar exhaustion, corresponding to 40 h and 48 h for *isu1Δ* and *ccc1Δ*, respectively (Fig. 4A).

Interestingly, although changes in expression of *isu1Δ* and *ssk2Δ* have started earlier in the fermentation when compared with the other mutants, *ccc1Δ* had a more similar temporal transcription profile to *isu1Δ* than the *ssk2Δ* mutant. Both deletions of *CCC1* and *ISU1* are known to increase the cytosolic amounts of Fe<sup>2+</sup> by different mechanisms: while *CCC1* deletion disables vacuole storage of Fe/Mn<sup>2+</sup>, *ISU1* deletion has a wider effect in the iron homeostasis, leading to constitutive activation of the transcription factors Aft1/2p, which controls a set of genes related to iron homeostasis. However, comparing *isu1Δ* and *ccc1Δ* strains at their start of xylose consumption (when both strains had consumed around 10 g l<sup>-1</sup>, corresponding to 16 and 24 h, respectively) to the control C5TY at its start of xylose consumption (48 h), deletion of *ISU1* generated a high expression (log<sub>2</sub>FC > 3) in genes related to stressful conditions, as heat shock proteins, that was not observed in *ccc1Δ* (data available on YeastC5 platform), suggesting that its deletion is more stressful than *CCC1* deletion, even though the strain resistance to oxidative stress was not affected (Fig. 2B and C).

In contrast, despite its faster xylose consumption and higher ethanol productivity when compared with C5TY, *bsd2Δ* did not show expressive differences in gene expression when compared with the corresponding time-point of the control.

#### *Temporal expression profile of isu1Δ indicates a metabolic remodelling in response to xylose*

Previous works have reported that yeasts engineered for xylose metabolism present under anaerobic conditions a respiratory response compared with glucose, which impairs xylose fermentation (Jin *et al.*, 2004). However, as our time-course fermentation data does indicate a fermentative response in the presence of xylose when compared with the control and a respiratory response is present only after xylose is depleted, we selected the *isu1Δ* strain to perform a complete temporal analysis of mRNA expression to understand the regulation of metabolic changes that had led to an increase in xylose consumption rates. To capture the full xylose fermentation profile, we collected six successive 8 h intervals samples over 48 h after *isu1Δ* start of fermentation and all time-point were compared with its first sample after inoculation (8 h) to perform the time-course analysis.

As metabolic changes in the glycolytic pathway are linked to sugar sensing (Conrad *et al.*, 2014), genes from the three main sugar signalling pathways (cAMP/PKA, Snf1/Mig1 and Snf3/Rgt2) were assessed (Fig. 5A). The SNF1 pathway, which is known to be expressed only in glucose-limited conditions, showed upregulation of the transcriptional activators involved in the metabolism of non-fermentable sugars, *CAT8* and *SIP4*, as well as their targets *FPB1*, *MLS1*, *ACS1* and *PCK1*, only after xylose depletion from the medium, suggesting that xylose was recognized as a fermentable sugar in this mutant.

Interestingly, *SUC2*, another glucose repressed gene encoding an invertase, showed its expression downregulated when compared with the control C5TY (data available on YeastC5 platform) and decreases its expression overall fermentation time (Fig. 5A). A recent study using a fluorescent biosensor coupled to the promoter region of *SUC2* showed that even high xylose concentrations (50 g l<sup>-1</sup>) fully induce its expression in the same manner that it does in low glucose conditions, whereas low C5 concentration (5 g l<sup>-1</sup>) slightly affect this biosensor (Osiro *et al.*, 2018). Curiously, our results showed that *SUC2* is downregulated even in the presence of xylose concentration (50 g l<sup>-1</sup>) when compared with the control C5TY (data available on YeastC5 platform), unlike reported with *SUC2*-biosensor. These results suggest that the presence of xylose in our mutant might mimics signals of glucose availability as it shows the genetic patterns of carbon catabolite repression in the presence of xylose. Additionally, the *HXK2* gene, which product is also known to be involved in *SNF1* inactivation and cooperates in the regulation of glucose-repressed genes (Conrad *et al.*, 2014), was upregulated at the beginning of fermentation, when the sugar was present, becoming downregulated only after 40 h, reinforcing an inactive SNF1 pathway in the presence of xylose in our strain *isu1Δ*. Curiously, the downregulation of *HXK2* at the end of fermentation was observed for all mutants, except for *bsd2Δ* (data available on YeastC5 platform).

Expression of *HXK2* is also related to an active PKA pathway (Conrad *et al.*, 2014). The genes required for intracellular PKA activation, *RAS1* and *CYR1*, as well as two catalytic subunits of PKA, *TPK1/2* genes, showed a decrease in expression throughout fermentation time, while the RAS/PKA inhibitor *IRA2* increased its expression only after xylose depletion. Decreased expression on *IRA2* was related to improve xylose consumption by constitutive activation of PKA (Myers *et al.*, 2019). This result suggests an active PKA in the *isu1Δ* strains at the beginning of fermentation, agreeing with the GO enrichments related to fermentation previously described.

Although these results suggest that xylose triggered in *isu1Δ* mutant similar metabolic changes as glucose, most of the hexose transporters maintained its expression



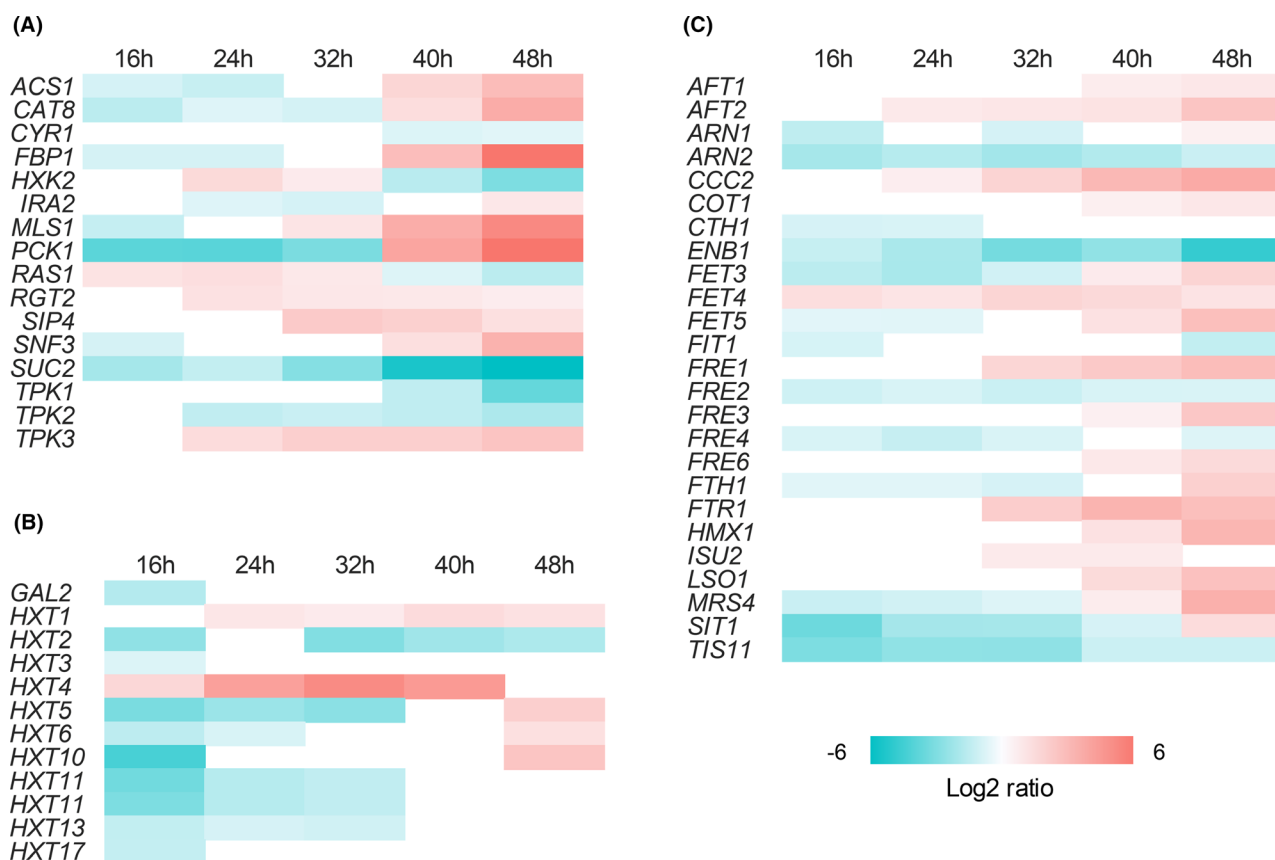


**Fig. 5.** Time-course profile of the sugar sensing, iron regulon and hexose transporters of *isu1Δ* during fermentation. Colours degrees show up (red) and downregulation (blue) of genes to average Log<sub>2</sub> fold change values of genes in each time-point compared with the sample of 8 h of *isu1Δ*. Genes of pathways from sugar sensing (A), hexose transporters (B) and Aft1/2p targets (C) are represented.

downregulated all long of fermentation, except for *HXT1* and *HXT4* (Fig. 5B). *HXT1* is a low-affinity glucose transporter which expression is induced under presence of glucose and, interestingly, its expression was also found in strains genetically modified to improve xylose consumption, harbouring the disruption of *IRA2* and *ISU1* genes (Osiro *et al.*, 2019).

Expression of hexose transporters in yeast is controlled by the sugar sensors Snf3p and Rgt2p in the presence of low and high glucose concentrations, respectively (Bisson *et al.*, 2016). These sugar sensors did not show high expression at the beginning of fermentation, suggesting that these sensors did not sense xylose as a fermentable sugar (Fig. 5A). This hypothesis agrees with the finding that, although cells cannot sense extracellular xylose, it responds towards intracellular xylose (Osiro *et al.*, 2018).

As *ISU1* is related to the control of metal homeostasis, we also examine genes involved in iron metabolism. Isu1p is a scaffold necessary for assembly of the mitochondrial iron-sulfur clusters (ISCs), which generates an intermediated compound, called (Fe-S)<sub>int</sub>, necessary for

production of the cytosolic ISCs by the cytosolic iron-sulfur cluster assembly (CIA) machinery (Pandey *et al.*, 2019). In conditions of iron sufficiency, cytosolic ISCs regulates the expression of the transcription factors Aft1/2p, which induces the expression of a set of genes in response to iron deprivation called the iron regulon (Fig. 6). Deletion of *ISU1*, as disruption of other genes of mitochondrial ISC assembly, has been reported to increase the mitochondrial iron content and constitutively activate the transcription factors Aft1/2p (Hausmann *et al.*, 2008; Lill *et al.*, 2014). Interestingly, although *isu1Δ* does have an increase in intracellular iron content (Fig. 2A), almost all Aft1/2p targets were downregulated at the beginning of fermentation (Fig. 5C). An alternative activation of the iron regulon relies on the connection between iron homeostasis and aerobic respiration (Casas *et al.*, 1997), and a regulatory connection between the main sugar signalling pathways and the iron regulon has been described. While an active cAMP/PKA pathway was described to inhibit Aft1 expression (Robertson *et al.*, 2000), the low-glucose sensing pathway Snf1/Mig1 is known to positively regulate Aft1/2p,

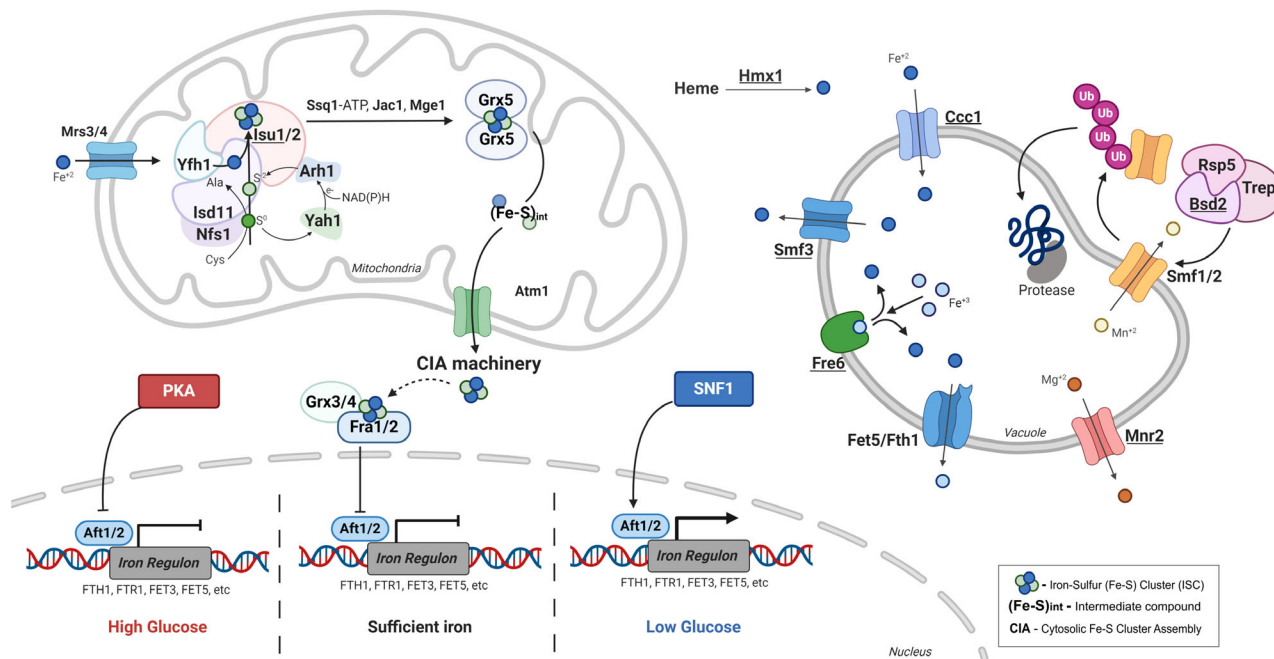


**Fig. 6.** Metabolic model of cellular metal homeostasis. *Isu1p* acts as a scaffold for mitochondrial iron-sulfur clusters (ISCs) assembly. In conditions of iron sufficiency, expression of the iron regulon is regulated by inhibition of the transcription factors *Aft1/2p*. The sugar sensing pathways *PKA* and *SNF1* also act on inhibition and activation of the iron regulon in conditions of high and low glucose, respectively. The vacuolar importer *Ccc1p* is expressed under high iron conditions to protect the cell against oxidative iron damage, while the genes *FRE6*, *HMX1*, *SMF3* and *FET5/FTH1* are activated by the iron regulon to prevent cell from iron starvation. The vacuolar exporter *Mnr2p* supply cells with magnesium from vacuole and *BSD2* encodes a protein necessary for vacuolar degradation of the heavy metal transporters *Smf1/2p*. Genes used in this study are underlined.

thus helping the switch from a fermentative to respiratory growth on glucose-limited conditions (Haurie *et al.*, 2003; Fig. 6). This result agrees with the sensing profile presented by *isu1Δ* and reinforces the evidence of *PKA* activation in the presence of xylose and activation of *SNF1/MIG1* pathway after xylose exhaustion.

## Conclusion

In this study, we explore different metabolisms associated with metal homeostasis and the non-obvious connection with improved xylose conversion rates into bioproducts. Our results point to *BSD2* and *CCC1* as promising novel targets to engineer *S. cerevisiae* towards xylose fermentation. Specific transcriptional responses point unique solutions for each mutant while a temporal transcriptional profile demonstrates a global metabolic reprogramming favouring the expression of essential genes for xylose metabolism and downregulation of a respiratory response. Although *S. cerevisiae* is not able to sense extracellular xylose, the engineered yeast demonstrated changes in gene expression patterns in the main sugar sensing signalling pathways.

## Experimental procedures

### Growth conditions

Yeast cells were cultured at 30°C in YP medium (10 g l<sup>-1</sup> yeast extract, 20 g l<sup>-1</sup> peptone) supplemented with 20 g l<sup>-1</sup> D-glucose as carbon source (YPD). For plates, 2% agar was added to the medium. Transformants were selected in YPD plates supplemented with 200 mg l<sup>-1</sup> of Hygromycin B or 200 mg l<sup>-1</sup> of geneticin.

Batch fermentations were performed in YP medium supplemented with 50 g l<sup>-1</sup> of xylose as the sole carbon source (YPX). The cultures started at an initial OD<sub>600</sub> of 1.0 and were incubated at 30°C and 200 rpm for 72 h. Fermentations were performed in biological triplicates using 100 ml sealed bottles containing a working volume of 70 ml. Samples for OD<sub>600</sub> measurements, extracellular metabolites and RNA sequencing were collected and stored at -20°C.

### Strains construction

The C5TY (C5-trial yeast) background strain used in this study was designed to express the complete xylose

pathway, including multi-copy integration of *xylA* and without any beneficial mutation fixed by adaptive evolution experiments. A MAT $\alpha$  haploid spore from PE-2 diploid strain was transformed with an additional copy of the genes xylulokinase (*XKS1*), transaldolase (*TAL1*), ribose-5-phosphate ketol-isomerase (*RKI1*), transketolase (*TKL1*), ribulose-5-phosphate 3-epimerase (*RPE1*) and the *xylA* gene from *Orpinomyces* sp. (Madhavan *et al.*, 2009) flanked by  $\delta$  LTR sequences, stably integrated at the *GRE3* locus under control of different strong constitutive promoters (Table S2). After adaptive evolution in xylose, the *xylA* gene was tandem amplified in 30 copies and a mutation Ser98Phe in *ISU1* gene was identified as responsible to improve xylose fermentation rates (personal communication). The mutation in *ISU1* was reverted to its original wild-type allele, resulting in the C5TY strain.

Strains with specific deletions (*bsd2 $\Delta$* , *ccc1 $\Delta$* , *isu1 $\Delta$* , *smf3 $\Delta$* , *ssk2 $\Delta$* , *mnr2 $\Delta$* , *fre6 $\Delta$* , *hmx1 $\Delta$* ) were created by PCR amplifying the hphMX6 cassette from plasmid pAG32 (Goldstein and McCusker, 1999), or the KanMX4 cassette (Wach *et al.*, 1994) from plasmid pFA6-kanMX4 for the double mutant *ccc1 $\Delta$ ssk2 $\Delta$* , with primers containing 42 bp homology to the upstream and downstream regions of target genes and then using the amplicon to delete genes on C5TY by homologous recombination *in vivo*. The transformation procedure was performed by lithium acetate using standard methods (Gietz and Schiestl, 2007) and all strains were confirmed for gene deletion by PCR with external flanking primers. Primers used for amplification and gene deletion confirmation are listed in Table S3.

#### Intracellular metal content analysis

Intracellular metal concentrations were analysed with an inductively coupled plasma optical emission spectrometer (ICP-OES, Optima™ 8000) using an adapted protocol from Eide *et al.* (2005). The yeast strains C5TY, *smf3 $\Delta$* , *bsd2 $\Delta$* , *ccc1 $\Delta$* , *isu1 $\Delta$*  and *ssk2 $\Delta$*  were grown in 100 ml of YPD medium at an initial OD<sub>600</sub> of 0.5 and incubated at 30°C, 200 rpm, overnight. The culture was collected by vacuum filtration using 0.2  $\mu$ m pore size membrane filters and cells were washed three times each with 30 ml of 1  $\mu$ M EDTA disodium salt solution, pH 8.0, followed by three additional washes with 30 ml of deionized water. Filtered cells were incubated at 65°C for 2 h to obtain the dry mass weight. Cells were then digested by microwave digestion (ETHOS™ Easy) through the addition of 14 ml of HNO<sub>3</sub> 2.0 M at each sample followed by 1.0 ml of H<sub>2</sub>O<sub>2</sub> 30% v/v, with a heating profile of 200°C over 20 min and then held in 200°C for 15 min, 1800 W. The final sample solution was then subjected to the measurements. A standard curve of 0.1–10.0 mg l<sup>-1</sup>

was prepared using a 1000 mg ml<sup>-1</sup> multi-element standard solution from PerkinElmer. All experiments were performed in triplicate.

#### Oxidative stress resistance on spot-assay growth

Cells grown overnight on YPD medium at 30°C and 200 rpm were harvested by centrifugation, washed three times, and suspended in sterile water at an initial OD<sub>600</sub> of 1.0 and serial-diluted to give concentrations of 10<sup>-1</sup>, 10<sup>-2</sup>, 10<sup>-3</sup> or 10<sup>-4</sup>. Samples (5  $\mu$ l) of each suspension were inoculated on solid YPD medium supplemented with 80 and 100  $\mu$ M of Menadione, 3 mM of H<sub>2</sub>O<sub>2</sub> or without supplementation. All experiments were made in triplicate and plates were incubated at 30°C for 48 h.

#### ROS assay by microscopy

ROS were measured using DHR (Sigma-Aldrich) with a protocol adapted from previously described reports (Madeo *et al.*, 1999; Peeters *et al.*, 2017). The yeast strains C5TY, *smf3 $\Delta$* , *bsd2 $\Delta$* , *ccc1 $\Delta$* , *isu1 $\Delta$*  and *ssk2 $\Delta$*  were grown overnight on YPD medium and menadione was added to a final concentration of 100  $\mu$ M in samples of each strain and incubated for 2 h at 30°C, 200 rpm. DHR was added to a final concentration of 10  $\mu$ g ml<sup>-1</sup> on each yeast sample and incubated for additional 2 h in the dark. Cells were pelleted and resuspended on 1  $\times$  PBS (137 mM NaCl, 2.7 mM KCl, 10 mM Na<sub>2</sub>HPO<sub>4</sub>, 1.8 mM KH<sub>2</sub>PO<sub>4</sub>) for microscopy visualization. Stained *S. cerevisiae* cells were visualized on fluorescence microscopy (Carl Zeiss, Jena, Germany) equipped with Compact Light Source HXP 120C (Jena, Germany) using the 100 $\times$  oil immersion objective lens. The captured images were further processed using AxioVision software version 3.1.

#### RNA extraction and library preparation

Cells for transcriptional analysis were harvested in biological triplicates at specific times from fermentation culture: all strains were collected at 8, 32, 40 and 48 h (*bsd2 $\Delta$* , *ccc1 $\Delta$* , *isu1 $\Delta$* , *ssk2 $\Delta$*  and C5TY), and additional samples were collected at 12 h for *isu1 $\Delta$*  and 24 h for the strains *ccc1 $\Delta$*  and *isu1 $\Delta$* . Total RNA was extracted using MasterPure™ Yeast RNA Purification Kit (Lucigen) according to the manufacturers' directions. The RNA integrity and purity were checked by Agilent RNA 6000 Nano kit on Agilent 2100 Bioanalyzer (Agilent) and the RNA quantity was determined by Qubit™ RNA BR Assay Kit (Thermo Fisher Scientific, MA, EUA), both following the manufacturer's protocols.

The RNA extracted was used to perform the Illumina® TruSeq Stranded mRNA Sample Prep (Low-Throughput

Protocol), according to the manufacturer's protocol. Library was validated by quality control using Agilent DNA 1000 kit on the 2100 Bioanalyzer (Agilent) and the DNA concentration was determined by qPCR using KAPA qPCR MasterMix (Roche) on the Vii7 Real-Time PCR System (Thermo Fisher Scientific). DNA template for cluster generation was prepared with the indexed DNA library normalized to 10 nM and then pooled. All libraries were made manually.

#### RNA analysis and data processing

The quality of the reads was assessed with FastQC (v.0.11.6) ([bioinformatics.babraham.ac.uk/projects/fastqc/](http://bioinformatics.babraham.ac.uk/projects/fastqc/)). Low-quality reads and adapters were removed by Trimmomatic (v. 0.38) with default parameters (Bolger *et al.*, 2014). SortMeRNA (v. 2.0) was used for rRNA filtering (Kopylova *et al.*, 2012). The reads were then mapped against the genome of *S. cerevisiae* strain LVY34.4 using the mapping tool STAR (v 2.14; Dobin *et al.*, 2013;), allowing the detection of splicing events. The BAM files generated by STAR were provided to BRAKER annotation tool (v. 1.8; Hoff *et al.*, 2019;), which combines the tools GeneMark-ET (v. 4.29) and AUGUSTUS (v. 3.1.0) and the aligned reads as evidence to generate full gene structure annotations. The functional annotation of the identified genes was carried with the webtool eggNOG-Mapper (standalone version; Huerta-Cepas *et al.*, 2017).

In order to quantify the transcript abundance the RSEM tool (v1.3.1) was employed with STAR as the mapping tool, and the genome of *S. cerevisiae* strain LVY34.4 and the transcriptome annotation generated by BRAKER as references. Differential expression analysis was made with the R package DESeq2 (v. 1.28.1; Love *et al.*, 2014), transcripts with  $FDR < 0.01$  and  $|\log_2FC| > 0.58$  between the compared groups were considered as differentially expressed. The RNA-Seq Illumina reads were deposited in the National Center for Biotechnology Information Short Read Archive (NCBI-SRA) and are publicly available under the accession number PRJNA708278 (BioProject ID).

#### YeastC5: A user-friendly application for transcriptome analysis

To facilitate transcriptome data visualization, an RNA-Seq bioinformatics tool was developed for a comprehensive automated analysis of the next-generation sequencing data produced in the time-course fermentations. The YeastC5 platform allows the user to explore the expression patterns of *isu1Δ*, *ccc1Δ*, *ssk2Δ* and *bsd2Δ* mutants intra and inter-strains compared with the C5TY control. Additionally, pathway plots can be explored for each

mutant for different primary metabolisms: aerobic respiration, glycolysis and gluconeogenesis, oxidative stress, PPP, TCA and glyoxylate cycles. The gene\_ID is unique and guides the individual analysis in a user-friendly interface. The application is available on <https://phybio.shinya.pps.io/YeastC5/>

#### Analytical procedures

The cellular growth was monitored by optical density (OD) measurements at a wavelength of 600 nm ( $OD_{600}$ ) using an Ultrospec 2100 Pro spectrophotometer (Amersham Biosciences). Quantification of xylose, xylitol, acetic acid, glycerol and ethanol in the cultures was determined via high-performance liquid chromatography using chromatograph Alliance (Waters) with refractive index detector (Waters 2414) using ion exclusion HPX-87H column ( $300 \times 7.8$  mm<sup>2</sup>, BioRad®), heated in an oven at 35°C, a 2 mM H<sub>2</sub>SO<sub>4</sub> solution as the mobile phase at a flow 0.6 ml min<sup>-1</sup>. A standard curve with known concentrations of compounds of interest was also analysed using the same procedure.

#### Acknowledgements

We thank Joice Janeri Gomes for Intracellular metal content analysis and Aline Tieppo Nogueira Mulato for RNA extraction and library preparation. This research used facilities of the Brazilian Biorenewables National Laboratory (LNBR), part of the Brazilian Center for Research in Energy and Materials (CNPEM), a private non-profit organization under the supervision of the Brazilian Ministry for Science, Technology, and Innovations (MCTI). The High Throughput Sequencing (NGS) staff is acknowledged for the assistance during the experiments of RNA sequencing. Figure 6 was created with BioRender.com.

#### Funding Information

This work was supported by Fundação de Amparo à Pesquisa do Estado de São Paulo (FAPESP, Grant Numbers: 2017/08519-6, 2018/00888-5, 2018/06254-8, 2020/07918-7), Conselho Nacional de Desenvolvimento Científico e Tecnológico (Grant Number: 430291/2018-3) and Serrapilheira Institute (Grant Number: Serra- 1708-16205). This study was financed in part by the Coordenação de Aperfeiçoamento de Pessoal de Nível Superior-Brasil (CAPES)—Finance Code 001.

#### Conflict of Interest

All authors declare that they have no conflict of interests.

## Author Contribution

**Gisele Cristina de Lima Palermo:** Investigation, Methodology, Visualization, Writing - Original Draft, Writing - Review & Editing. **Natalia Coutoné:** Data Curation, Writing - Original Draft. **João Gabriel Ribeiro Bueno:** Investigation, Writing - Original Draft. **Lucas Ferreira Maciel:** Software, Data Curation, Visualization. **Leandro Vieira dos Santos:** Conceptualization, Methodology, Supervision, Visualization, Project administration, Writing - Original Draft, Writing - Review & Editing, Funding acquisition.

## Data Availability Statement

The sequence data have been submitted to the NCBI-SRA and are publicly available under the accession number PRJNA708278 (BioProject ID). Datasets related to this article can be found at <https://phybio.shinyapps.io/YeastC5/>

## References

- Attfeld, P.V. (1997) Stress tolerance: the key to effective strains of industrial baker's yeast. *Nat Biotechnol* **15**: 1351–1357.
- Bisson, F.L., Fan, Q., and Walker, G.A. (2016) Sugar and Glycerol Transport in *Saccharomyces cerevisiae*. *Yeast Membrane Transport*. Ramos, J., Sychrová, H., and Kschischo, M. (eds). Cham: Springer International Publishing, pp. 125–168. [https://doi.org/10.1007/978-3-319-25304-6\\_6](https://doi.org/10.1007/978-3-319-25304-6_6)
- Bolger, A.M., Lohse, M., and Usadeln, B. (2014) Trimmomatic: a flexible trimmer for Illumina sequence data. *Bioinformatics* **30**: 2114–2120. <http://dx.doi.org/10.1093/bioinformatics/btu170>.
- Bueno, J.G.R., Borelli, G., Corrêa, T.L.R., Fiamenghi, M.B., José, J., de Carvalho, M., *et al.* (2020) Novel xylose transporter Cs4130 expands the sugar uptake repertoire in recombinant *Saccharomyces cerevisiae* strains at high xylose concentrations. *Biotechnol Biofuels* **13**: 145.
- Casas, C., Aldea, M., Espinet, C., Gallego, C., Gil, R., and Herrero, E. (1997) The AFT1 transcriptional factor is differentially required for expression of high-affinity iron uptake genes in *Saccharomyces cerevisiae*. *Yeast* **13**: 621–637.
- Chen, Y., Li, F., Mao, J., Chen, Y., and Nielsen, J. (2021) Yeast optimizes metal utilization based on metabolic network and enzyme kinetics. *Proc Natl Acad Sci USA* **118**: e2020154118.
- Conrad, M., Schothorst, J., Kankipati, H.N., Van Zeebroeck, G., Rubio-Teixeira, M., and Thevelein, J.M. (2014) Nutrient sensing and signaling in the yeast *Saccharomyces cerevisiae*. *FEMS Microbiol Rev* **38**: 254–299.
- Dobin, A., Davis, C.A., Schlesinger, F., Drenkow, J., Zaleski, C., Jha, S., *et al.* (2013) STAR: Ultrafast universal RNA-seq aligner. *Bioinformatics* **29**: 15–21.
- dos Santos, L.V., Carazzolle, M.F., Nagamatsu, S.T., Sampaio, N.M.V., Almeida, L.D., Pirolla, R.A.S., *et al.* (2016) Unraveling the genetic basis of xylose consumption in engineered *Saccharomyces cerevisiae* strains. *Sci Rep* **6**: 38676.
- Eide, D.J., Clark, S., Nair, T.M., Gehl, M., Gribskov, M., Guerinot, M.L., and Harper, J.F. (2005) Characterization of the yeast ionome: a genome-wide analysis of nutrient mineral and trace element homeostasis in *Saccharomyces cerevisiae*. *Genome Biol* **6**: Article R77. <https://doi.org/10.1186/gb-2005-6-9-r77>.
- Garland, S.A., Hoff, K., Vickery, L.E., and Culotta, V.C. (1999) *Saccharomyces cerevisiae* ISU1 and ISU2: Members of a well-conserved gene family for iron-sulfur cluster assembly. *J Mol Biol* **294**: 897–907.
- Gietz, R.D., and Schiestl, R.H. (2007) Large-scale high-efficiency yeast transformation using the LiAc/SS carrier DNA/PEG method. *Nat Protoc* **2**: 38–41.
- Goldstein, A.L., and McCusker, J.H. (1999) Three new dominant drug resistance cassettes for gene disruption in *Saccharomyces cerevisiae*. *Yeast* **15**: 1541–1553.
- Haurie, V., Boucherie, H., and Sagliocco, F. (2003) The Snf1 protein kinase controls the induction of genes of the iron uptake pathway at the diauxic shift in *Saccharomyces cerevisiae*. *J Biol Chem* **278**: 45391–45396.
- Hausmann, A., Samans, B., Lill, R., and Mühlenhoff, U. (2008) Cellular and mitochondrial remodeling upon defects in iron-sulfur protein biogenesis. *J Biol Chem* **283**: 8318–8330.
- Hoff, K.J., Lomsadze, A., Borodovsky, M., and Stanke, M. (2019) Whole-genome annotation with BRAKER. *Methods Mol Biol* **1962**: 65–95.
- Huerta-Cepas, J., Forslund, K., Coelho, L.P., Szklarczyk, D., Jensen, L.J., von Mering, C., and Bork, P. (2017) Fast genome-wide functional annotation through orthology assignment by eggNOG-Mapper. *Mol Biol Evol* **34**: 2115–2122.
- Jin, Y.-S., Laplaza, J.M., and Jeffries, T.W. (2004) *Saccharomyces cerevisiae* engineered for xylose metabolism exhibits a respiratory response. *Appl Environ Microbiol* **70**: 6816–6825.
- Kopylova, E., Noé, L., and Touzet, H. (2012) SortMeRNA: fast and accurate filtering of ribosomal RNAs in metatranscriptomic data. *Bioinformatics* **28**: 3211–3217.
- Kovalevsky, A.Y., Hanson, L., Fisher, S.Z., Mustyakimov, M., Mason, S.A., Trevor Forsyth, V., *et al.* (2010) Metal Ion roles and the movement of hydrogen during reaction catalyzed by D-xylose isomerase: a joint X-ray and neutron diffraction study. *Structure* **18**: 688–699.
- Kwak, S., and Jin, Y.-S. (2017) Production of fuels and chemicals from xylose by engineered *Saccharomyces cerevisiae*: a review and perspective. *Microb Cell Fact* **16**: 82.
- Laviña, W.A., Shahsavarian, H., Saidi, A., Sugiyama, M., Kaneko, Y., and Harashima, S. (2014) Suppression mechanism of the calcium sensitivity in *Saccharomyces cerevisiae* ptp2Δmsg5Δ double disruptant involves a novel HOG-independent function of Ssk2, transcription factor Msn2 and the protein kinase A component Bcy1. *J Biosci Bioeng* **117**: 135–141.
- Lee, M., Rozeboom, H.J., de Waal, P.P., de Jong, R.M., Dudek, H.M., and Janssen, D.B. (2017) Metal

- dependence of the xylose isomerase from *Piromyces* sp. E2 explored by activity profiling and protein crystallography. *Biochemistry* **56**: 5991–6005.
- Lee, M., Rozeboom, H.J., Keuning, E., de Waal, P., and Janssen, D.B. (2020) Structure-based directed evolution improves *S. cerevisiae* growth on xylose by influencing in vivo enzyme performance. *Biotechnol Biofuels* **13**: 5.
- Li, L., Chen, O.S., Ward, D.M.V., and Kaplan, J. (2001) CCC1 is a transporter that mediates vacuolar iron storage in yeast. *J Biol Chem* **276**: 29515–29519.
- Li, L., Jia, X., Ward, D.M., and Kaplan, J. (2011) Yap5 protein-regulated transcription of the TYW1 gene protects yeast from high iron toxicity. *J Biol Chem* **286**: 38488–38497.
- Li, X., Park, A., Estrela, R., Kim, S.-R., Jin, Y.-S., and Cate, J.H.D. (2016) Comparison of xylose fermentation by two high-performance engineered strains of *Saccharomyces cerevisiae*. *Biotechnol Reports* **9**: 53–56.
- Lill, R., Srinivasan, V., and Mühlenhoff, U. (2014) The role of mitochondria in cytosolic-nuclear iron–sulfur protein biogenesis and in cellular iron regulation. *Curr Opin Microbiol* **22**: 111–119.
- Liu, X.F., Supek, F., Nelson, N., and Culotta, V.C. (1997) Negative control of heavy metal uptake by the *Saccharomyces cerevisiae* BSD2 gene. *J Biol Chem* **272**: 11763–11769.
- Love, M.I., Huber, W., and Anders, S. (2014) Moderated estimation of fold change and dispersion for RNA-seq data with DESeq2. *Genome Biol* **15**: 550.
- Madeo, F., Fröhlich, E., Ligr, M., Grey, M., Sigrist, S.J., Wolf, D.H., and Fröhlich, K.U. (1999) Oxygen stress: A regulator of apoptosis in yeast. *J Cell Biol* **145**: 757–767.
- Madhavan, A., Tamalampudi, S., Ushida, K., Kanai, D., Katahira, S., Srivastava, A., *et al.* (2009) Xylose isomerase from polycentric fungus *Orpinomyces*: gene sequencing, cloning, and expression in *Saccharomyces cerevisiae* for bioconversion of xylose to ethanol. *Appl Microbiol Biotechnol* **82**: 1067–1078.
- Martínez-Pastor, M.T., Perea-García, A., and Puig, S. (2017) Mechanisms of iron sensing and regulation in the yeast *Saccharomyces cerevisiae*. *World J Microbiol Biotechnol* **33**: 75.
- Martins, L.J., Jensen, L.T., Simons, J.R., Keller, G.L., and Winge, D.R. (1998) Metalloregulation of FRE1 and FRE2 homologs in *Saccharomyces cerevisiae*. *J Biol Chem* **273**: 23716–23721.
- Martins, T.S., Pereira, C., Canadell, D., Vilaça, R., Teixeira, V., Moradas-Ferreira, P., *et al.* (2018) The Hog1p kinase regulates Aft1p transcription factor to control iron accumulation. *Biochim Biophys Acta - Mol Cell Biol Lipids* **1863**: 61–70.
- Morano, K.A., Grant, C.M., and Moye-Rowley, W.S. (2012) The response to heat shock and oxidative stress in *Saccharomyces cerevisiae*. *Genetics* **190**: 1157–1195.
- Moyes, D., Reis, V., Almeida, J., Moraes, L., and Torres, F. (2016) Xylose fermentation by *Saccharomyces cerevisiae*: challenges and prospects. *Int J Mol Sci* **17**: 207.
- Mühlenhoff, U., Molik, S., Godoy, J.R., Uzarska, M.A., Richter, N., Seubert, A., *et al.* (2010) Cytosolic monothiol glutaredoxins function in intracellular iron sensing and trafficking via their bound iron-sulfur cluster. *Cell Metab* **12**: 373–385.
- Myers, K.S., Riley, N.M., MacGilvray, M.E., Sato, T.K., McGee, M., Heilberger, J., *et al.* (2019) Rewired cellular signaling coordinates sugar and hypoxic responses for anaerobic xylose fermentation in yeast. *PLOS Genet* **15**: e1008037.
- Osiro, K.O., Borgström, C., Brink, D.P., Fjölfnisdóttir, B.L., and Gorwa-Grauslund, M.F. (2019) Exploring the xylose paradox in *Saccharomyces cerevisiae* through in vivo sugar signalomics of targeted deletants. *Microb Cell Fact* **18**: 88.
- Osiro, K.O., Brink, D.P., Borgström, C., Wasserstrom, L., Carlquist, M., and Gorwa-Grauslund, M.F. (2018) Assessing the effect of d-xylose on the sugar signaling pathways of *Saccharomyces cerevisiae* in strains engineered for xylose transport and assimilation. *FEMS Yeast Research* **18**: fox096.
- Pandey, A.K., Pain, J., Dancis, A., and Pain, D. (2019) Mitochondria export iron-sulfur and sulfur intermediates to the cytoplasm for iron-sulfur cluster assembly and tRNA thiolation in yeast. *J Biol Chem* **294**: 9489–9502.
- Peeters, K., Van Leemputte, F., Fischer, B., Bonini, B.M., Quezada, H., Tsytlonok, M., *et al.* (2017) Fructose-1,6-bisphosphate couples glycolytic flux to activation of Ras. *Nat Commun* **8**: 922.
- Pisat, N.P., Pandey, A., and MacDiarmid, C.W. (2009) MNR2 regulates intracellular magnesium storage in *Saccharomyces cerevisiae*. *Genetics* **183**: 873–884.
- Portnoy, M.E., Liu, X.F., and Culotta, V.C. (2000) *Saccharomyces cerevisiae* expresses three functionally distinct homologues of the nramp family of metal transporters. *Mol Cell Biol* **20**: 7893–7902.
- Protchenko, O., and Philpott, C.C. (2003) Regulation of intracellular heme levels by HMX1, a homologue of heme oxygenase, in *Saccharomyces cerevisiae*. *J Biol Chem* **278**: 36582–36587.
- Qi, X., Zha, J., Liu, G.-G., Zhang, W., Li, B.-Z., and Yuan, Y.-J. (2015) Heterologous xylose isomerase pathway and evolutionary engineering improve xylose utilization in *Saccharomyces cerevisiae*. *Front Microbiol* **6**: 1165.
- Robertson, L.S., Causton, H.C., Young, R.A., and Fink, G.R. (2000) The yeast A kinases differentially regulate iron uptake and respiratory function. *Proc Natl Acad Sci USA* **97**: 5984–5988.
- Saito, H., and Posas, F. (2012) Response to hyperosmotic stress. *Genetics* **192**: 289–318.
- Sato, T.K., Tremaine, M., Parreiras, L.S., Hebert, A.S., Myers, K.S., Higbee, A.J., *et al.* (2016) Directed evolution reveals unexpected epistatic interactions that alter metabolic regulation and enable anaerobic xylose use by *Saccharomyces cerevisiae*. *PLOS Genet* **12**: e1006372.
- Sharma, H.K., Xu, C., and Qin, W. (2019) Biological Pretreatment of Lignocellulosic Biomass for Biofuels and Bioproducts: An Overview. *Waste and Biomass Valorization* **10**: 235–251. <http://dx.doi.org/10.1007/s12649-017-0059-y>.
- Verhoeven, M.D., Lee, M., Kamoen, L., van den Broek, M., Janssen, D.B., Daran, J.-M., *et al.* (2017) Mutations in PMR1 stimulate xylose isomerase activity and anaerobic growth on xylose of engineered *Saccharomyces*

- cerevisiae* by influencing manganese homeostasis. *Sci Rep* **7**: 46155.
- Wach, A., Brachat, A., Pöhlmann, R., and Philippsen, P. (1994) New heterologous modules for classical or PCR-based gene disruptions in *Saccharomyces cerevisiae*. *Yeast* **10**: 1793–1808.
- Wagner, E.R., Myers, K.S., Riley, N.M., Coon, J.J., and Gasch, A.P. (2019) PKA and HOG signaling contribute separable roles to anaerobic xylose fermentation in yeast engineered for biofuel production. *PLoS One* **14**: e0212389.
- Yu, D., Danku, J.M.C., Baxter, I., Kim, S., Vatamaniuk, O.K., Vitek, O., *et al.* (2012) High-resolution genome-wide scan of genes, gene-networks and cellular systems impacting the yeast ionome. *BMC Genom* **13**: 623.
- Zhou, H., Cheng, J., Wang, B.L., Fink, G.R., and Stephanopoulos, G. (2012) Xylose isomerase overexpression along with engineering of the pentose phosphate pathway and evolutionary engineering enable rapid xylose utilization and ethanol production by *Saccharomyces cerevisiae*. *Metab Eng* **14**: 611–622.